1,2-Dihydrophosphete: A Platform for the Molecular Engineering of Electroluminescent Phosphorus Materials for Light-Emitting Devices

ARTICLE *in* CHEMISTRY · JULY 2014

Impact Factor: 5.93 · DOI: 10.1002/chem.201400050 · Source: PubMed

12 AUTHORS, INCLUDING:

Pierre-Antoine Bouit

Université de Rennes 1

39 PUBLICATIONS **774** CITATIONS

SEE PROFILE

Bernard Geffroy

Atomic Energy and Alternative Energies Co…

114 PUBLICATIONS **1,110** CITATIONS

SEE PROFILE

Régis Réau

Université de Rennes 1

154 PUBLICATIONS **3,953** CITATIONS

SEE PROFILE

Muriel Hissler

Université de Rennes 1

71 PUBLICATIONS **2,785** CITATIONS

SEE PROFILE

ChemPubSoc Europe

DOI: 10.1002/chem.201400050

CHEMISTRY
A European Journal
Full Paper

Phosphorus Heterocycles

1,2-Dihydrophosphete: A Platform for the Molecular Engineering of Electroluminescent Phosphorus Materials for Light-Emitting Devices

Hui Chen,[b] Simon Pascal,[a] Zuoyong Wang,[b] Pierre-Antoine Bouit,[a] Zisu Wang,[b] Yinlong Zhang,[b] Denis Tondelier,[e] Bernard Geffroy,[d] Régis Réau,*[a] François Mathey,*[b, c] Zheng Duan,*[b] and Muriel Hissler*[a]

Abstract: The discovery and molecular engineering of novel electroluminescent materials is still a challenge in optoelectronics. In this work, the development of new π-conjugated oligomers incorporating a dihydrophosphete skeleton is reported. Variation of the substitution pattern of 1,2-dihydrophosphete derivatives and chemical modification of their P atoms afford thermally stable derivatives, which are suitable emitters to construct organic light-emitting diodes (OLEDs). The optical and electrochemical properties of these new P-based oligomers have been investigated in detail and are supported by DFT calculations. The OLED devices exhibit good performance and current-independent CIE coordinates.

Introduction

Organic light-emitting diodes (OLEDs) are key devices in the development of flat and flexible organic electronics. They have already been commercialized as components for displays and they have the potential for other promising applications such as solid-state lighting.[1] Despite the great success achieved by some commercial products in this area, the discovery and molecular engineering of novel electroluminescence-emitting materials with improved electrical and optical properties are still relevant. With this aim, various heterocyclopentadienes (thiophene, silole, and so forth) have been incorporated into the backbone of π-conjugated systems, since their electronic properties are dependent on the nature of the heteroatom. For example, phospholes (molecule **B**, Figure 1) have received particular attention as building blocks for the tailoring of functional π-conjugated systems for optoelectronic applications.[2] One appealing property of this five-membered heterocycle is that simple chemical modifications of the reactive phosphorus center allow tuning of the HOMO and LUMO levels, improvement of the thermal stability, and control of the solid-state organization of the π systems, thereby providing a simple and direct method for diversifying the structure and properties. This unique way of π-system molecular engineering afforded efficient materials for OLEDs, including white-emitting devices.[3] These results prompted us to prepare and study the physical properties of other phosphacycles as building blocks for electroluminescent π-conjugated materials. Phosphorus heterocyclic chemistry is nowadays well developed and many types of π derivatives (four-, five-, six-, and seven-membered rings; presence of several heteroatoms; see Figure 1) are easily available on the gram scale.[4]

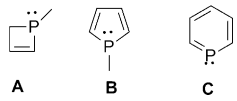

Figure 1. Phosphorus heterocycles: 1,2-dihydrophosphete (A), phosphole (B), phosphinine (C).

Among this diversity of structures, we focused on the 1,2-dihydrophosphete skeleton (molecule **A**, Figure 1) for the development of π-conjugated materials for several reasons. This unsaturated building block has been known since the 1980s, and

[a] *S. Pascal, Dr. P.-A. Bouit, Prof. R. Réau, Prof. M. Hissler*
Institut des Sciences Chimiques de Rennes
UMR6226 CNRS-Université de Rennes 1
Campus de Beaulieu, 35042 Rennes Cedex (France)
E-mail: regis.reau@uni-rennes1.fr
mhissler@univ-rennes1.fr

[b] *H. Chen, Z. Wang, Z. Wang, Y. Zhang, Prof. F. Mathey, Prof. Z. Duan*
College of Chemistry and Molecular Engineering
International Phosphorus Laboratory
Joint Research Laboratory for Functional Organophosphorus Materials of Henan Province
Zhengzhou University, Zhengzhou 450001 (P. R. China)
E-mail: fmathey@ntu.edu.sg
duanzheng@zzu.edu.cn

[c] *Prof. F. Mathey*
Nanyang Technological University, CBC-SPMS
21 Nanyang Link, Singapore 637371 (Singapore)

[d] *B. Geffroy*
Laboratoire de Chimie des Surfaces et Interfaces
CEA Saclay, IRAMIS, SPCSI
91191 Gif-sur-Yvette Cedex (France)

[e] *D. Tondelier*
Laboratoire de Physique des Interfaces et Couches Minces
CNRS UMR 7647, Ecole Polytechnique
91128 Palaiseau (France)

Supporting information for this article is available on the WWW under http://dx.doi.org/10.1002/chem.201400050.

its synthesis and reactivity have been widely investigated making this type of heterocycle easily accessible and well understood.[5] Within this family of P rings, the 2-(diphenylmethylene)-1,4-diphenyl-1,2-dihydrophosphete skeleton (molecule **2a**–**f**, Scheme 1) appeared to us as an original platform for the development of novel P materials for optoelectronic applications. Firstly, it possesses a π-conjugated system interacting with a phosphorus atom within a four-membered unsaturated ring. It was thus of interest to investigate the impact of P modifications for tuning the electronic properties of this π system. Note that the optical and electrochemical properties of this family of P heterocycles have never been investigated. Secondly, the pyramidal shape of the P atom affords steric hindrance, which is a key parameter for solid-state engineering of chromophores since it should prevent the aggregation phenomena from taking place. Lastly, straightforward synthesis of phosphetes allowing easy derivatization is known and these rings appear to exhibit quite high chemical and thermal stability.

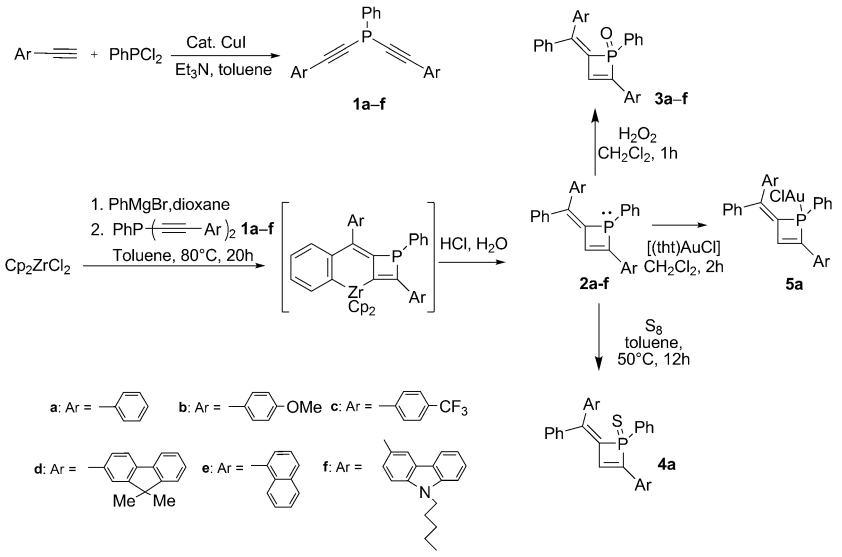

Scheme 1. Synthesis of the 1,2-dihydrophosphete derivatives. Cp = cyclopentadienyl.

Herein, we report on the synthesis of a new family of 1,2-dihydrophosphete derivatives **3a**–**f**, **4a**, and **5a** (Scheme 1) and the elucidation of their photophysical, thermal, and electrochemical properties by following UV/Vis, photoluminescence, cyclic voltammetry, thermogravimetric analysis (TGA), and differential scanning calorimetry (DSC) studies. The use of these P rings as emitting materials in OLED devices is reported. These devices emit in the blue–green region, thus illustrating the potential of this novel P platform for the development of materials for molecular electronics.

Results and Discussion

1,2-Dihydrophosphete derivatives **2a**–**f** were synthesized according to a straightforward one-pot, four-step procedure devised by Majoral et al.[5e] (Scheme 1), involving an intramolecular coupling reaction of a dialkynylphosphane and zirconocene-benzene. The starting materials **1a**–**f** (^{31}P NMR: δ = ca. −60 ppm) were obtained in medium to good yields (47–83%) through copper-catalyzed cross-coupling of terminal alkynes with dichlorophenylphosphine (Scheme 1).[6] The presence of the Ph substituents on the P atom is essential for providing good solubility and stability to these derivatives. They were reacted with the transient benzyne complex, generated in situ by thermolysis of a solution of [Cp_2ZrPh_2] in toluene at 80 °C, which resulted in the formation of the corresponding benzo-zirconacyclohexadiene-phosphabutenes, which, upon treatment in acidic media, gave access to the expected 1,2-dihydrophosphetes **2a**–**f** (^{31}P NMR: δ = ca. +22.0 ppm; Scheme 1).[5e–g] The trivalent P atom of 1,2-dihydrophosphetes is sensitive to oxidation, so they were readily transformed into the σ^4 derivatives **3a**–**f**, **4a**, and **5a** by treatment with hydrogen peroxide, elemental sulfur, and (tht)AuCl, respectively (tht = tetrahydrothiophene; Scheme 1).[2] These compounds were purified by column chromatography and isolated as air-stable powders in good yields (34–58%). The newly prepared P compounds **1b**–**f**, **3a**–**f**, **4a**, and **5a** were characterized by high-resolution mass spectrometry and elemental analysis, and their multinuclear NMR spectroscopic data support the proposed structures. It is noteworthy that this synthetic route is rather simple and efficient, allowing both gram-scale preparation and introduction of a large variety of functional groups (electron-withdrawing and electron-donating substituents) on the organophosphorus backbone through functionalization of the starting dialkynylphosphanes **1** (Scheme 1). Furthermore, P functionalization allows additional straightforward derivatization (P=O, P=S, P–AuCl) of these π-conjugated platforms.

The structure of the gold complex **5a** was investigated by X-ray crystallography to gain insight into the organization of the phosphete derivatives in the solid state (Figure 2). Single crystals of **5a** suitable for X-ray diffraction study were grown upon diffusion of pentane into a dichloromethane solution. The metric data of the phosphete–AuCl subunit are classical (Table 1).[3e] For example, the phosphorus center adopts a distorted tetrahedral geometry (ΣP_{ang} = 294.8°) and the endocyclic P–C bond lengths (1.830(6) Å, Table 1) approach that of a P–C single bond (1.84 Å). The geometry around the Au atom is almost linear (P-Au-Cl, 178.69(6)°). The π-conjugated backbone including the dihydrophosphete ring and the substituents in positions 2 and 4 (exocyclic double bond and phenyl

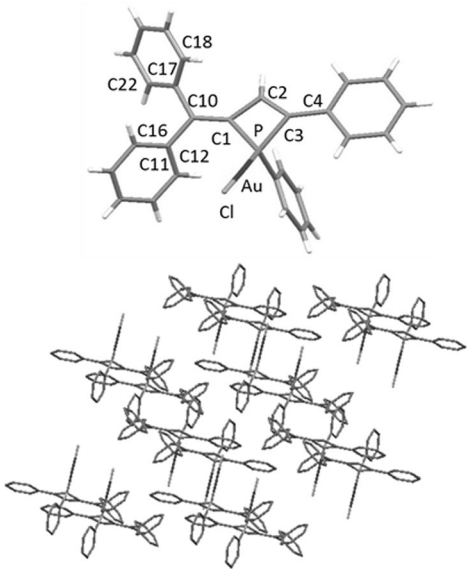

Figure 2. Structure and packing of the gold complex **5a** in the solid state.

Table 1. Selected bond lengths and twist angles between the phosphete ring and its 2- and 4-substituents for the gold complex **5a**.

Bond length [Å]		Angle [°]	
P–C1	1.830(6)	C1-P-C3	74.5(3)
C1–C2	1.462(9)	C1-P-C23	115.2(2)
C2–C3	1.363(8)	C1-P-Au	119.4(2)
C3–P	1.829(6)	C3-P-C23	107.3(3)
P–Au	2.2237(19)	C3-P-Au	120.9(2)
Au–Cl	2.291(2)	C23-P-Au	115.2(2)
C1–C10	1.349(8)	P-Au-Cl	178.69(7)
C3–C4	1.455(8)	–	–

ring) are planar (maximum deviation from the mean C-sp^2 plane, 0.06 Å) and the C–C bond lengths (d_{C3-C4} = 1.455(8) Å, d_{C1-C2} = 1.462(9) Å, Figure 2) between the double bonds are in the range expected for (C(sp^2)–C(sp^2)) single bonds. These data indicate the presence of an extended π conjugation including the endocyclic double bond of the phosphete and the substituents in the 2- and 4-positions (exocyclic double bond and phenyl ring). Note that the two lateral phenyl substituents of the C10 atom (Figure 2) are twisted with respect to this main C-sp^2 plane (twist angles 44.2 and 59.2°) due to H–H repulsion.

The solid-state organization of complex **5a** (Figure 2) shows no intermolecular π–π, CH–π, or aurophilic (d(Au–Au) > 5.3 Å) interactions. This property is most likely due to the presence of substituents out of the C-sp^2 planes (P- and C10-phenyl substituents), which provide steric hindrance. This property is promising in the prospect of using these compounds as emitters in OLEDs since aggregation of emitting materials is known to reduce the efficiency of these devices.

To establish the structure–property relationship for this novel series of P-based π-conjugated systems (Scheme 1), their UV/Vis absorption, excitation, and fluorescence spectra were measured in CH_2Cl_2 (Table 2). Notably, the polarity and the hydrogen-bond donor ability of the solvent have a negligible effect on the absorption and emission properties and the UV/Vis absorption maxima are in very good agreement with the excitation data (see Figures S1–S4 in the Supporting Information).

Compounds **3**–**5a** display an intense band in the UV/Vis region centered at 358 nm, attributed to π–π* transitions of the extended π-conjugated system including the dihydrophosphete ring and substituents in positions 2 and 4 (exocyclic double bond and phenyl ring). Interestingly, these derivatives exhibit blue emissions (Figure 3) albeit with low quantum yields (Φ_f = 0.5–12.4%, Table 2). The presence of the "bridging phosphorus atom" impacts the optical properties compared to the 1,1,4-triphenylbutadiene.[7] Due to a partial rigidification of the π system, redshifted structured absorption and emission bands are observed for the dihydrophosphete compound, which suggests a better electron delocalization along the π system and a small rearrangement of these molecules upon photoexcitation. In return, the substituent on the P atom has a very weak impact on the optical transitions but clearly impacts the quantum yield, with best performance for the P=O derivative **3a** (Table 2). Interestingly, the introduction of electron-rich substituents (**3b**) induces a bathochromic shift of absorption and emission maxima whereas the introduction of electron-deficient substituents (**3c**) has no impact on the opti-

Table 2. Photophysical, electrochemical, and thermal data for **3a**–**f**, **4a**, and **5a**.

Compound	λ_{max} [nm][a]	ε [$M^{-1}cm^{-1}$]	λ_{em} [nm][a]	Φ_f [%][b]	T_{TGA} [°C][c]	T_m [°C][d]	E^1_{ox} [V][e]	E^1_{red} [V][e]
3a	358	36900	426	2.4	316	205	–[g]	−2.19
3b	375	36800	445	1.6	320	75	+0.76[f]	–[g]
3c	360	30100	426	0.6	300	165	–[g]	−1.87[f]
3d	400	50000	458/480	6.6	375	230	+0.79[f]	−2.09[f]
3e	375	33200	456	5.2	340	–[g]	+1.19	−2.14
3f	409	36200	483	12.4	345	–[g]	+0.49[f]	−2.46
4a	358	27700	421	0.5	330	152	+1.03	−2.13[f]
5a	359	33200	425	0.9	300	130	+1.15	−2.09

[a] Measured in CH_2Cl_2 (5×10^{-5} M). [b] Measured relative to quinine sulfate (H_2SO_4, 0.1 M), ±15%. [c] Onset weight-loss temperature estimated using TGA under nitrogen. [d] Melting point measured by DSC under argon, 10 °C min^{-1}. [e] All potentials were obtained during cyclic voltammetric investigations in 0.2 M Bu_4NPF_6 in CH_2Cl_2. Platinum electrode diameter 1 mm, sweep rate 200 mV s^{-1}. All potentials are referenced to the reversible formal potential of ferrocene/ferrocenium (Fc/Fc^+). [f] Reversible process. [g] Not observed.

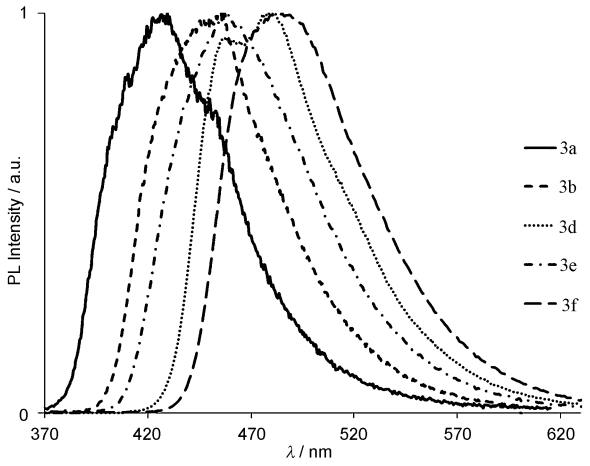

Figure 3. Normalized photoluminescence (PL) emission spectra of **3a**, **3b**, and **3d**–**f** recorded in dichloromethane (5×10^{-6} M).

cal properties. This effect is attributed to an intramolecular charge transfer from the electron-donating group to the electron-deficient dihydro-oxophosphete center. Moreover, upon extension of the π-conjugated system, all optical features are significantly redshifted from those of compound **3a** (Table 2). The smallest bathochromic shift is observed with the naphthalene-substituted oligomer **3e** ($\lambda_{abs}=375$ nm, $\lambda_{em}=456$ nm). The fluorene- and carbazole-substituted oligomers (**3d**, **3f**) show significantly redshifted maxima of absorption and emission (**3d**, $\lambda_{abs}=400$ nm, $\lambda_{em}=468$ nm; **3f**, $\lambda_{abs}=409$ nm, $\lambda_{em}=483$ nm), which indicate an increased effective conjugation length in both molecules relative to compound **3a**. Furthermore, compounds **3d**–**f** display an emission band in the 460–480 nm range with moderate quantum yield in solution ($5\%<\Phi_f<12\%$), thus making them a good candidate to act as blue emitter in OLED devices.

To gain a deeper understanding of the electronic structure of these phosphete derivatives (Figure 4), DFT calculations at

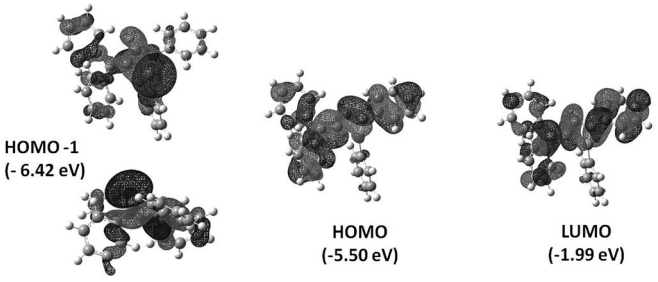

Figure 4. Calculated molecular orbital amplitude plots of HOMO−1, HOMO, and LUMO levels of **2a**.

the B3LYP/6-31+G(d,p) level were carried out to obtain orbital distributions of the highest occupied molecular orbitals (HOMO, HOMO−1) and the lowest unoccupied molecular orbital (LUMO) energy levels. As shown in Figure 4, the calculated optimized structure of derivative **2a** shows that the π-conjugated backbone, including the dihydrophosphete ring and substituents in positions 2 and 4 (exocyclic double bond and phenyl ring), is planar and is similar to the structure of **5a** (Figure 2). The HOMO and LUMO energy levels are localized on the entire π-conjugated carbon framework and the contribution of the phosphorus lone pair is mainly localized in the HOMO−1. The difference in energy between the HOMO−1 and HOMO is significant and neither the HOMO nor the LUMO shows a sizeable localization at phosphorus, therefore the chemical modifications on the phosphorus atom will have negligible impact on the HOMO–LUMO gap, as observed by UV/Vis absorption.

The impact of these chemical modifications performed on the P atom (**3a**) or on the π system by introduction of electron-rich or -deficient substituents (**3b** and **3c**, respectively) on the molecular orbital levels has also been rationalized by DFT calculations. As observed for **2a** (see above), the computed molecular orbitals of **3a**–**c** are fully delocalized over the entire backbone. The oxidation of the P atom induces a stabilization of the molecular orbital levels as well as a reduction of the HOMO–LUMO gap (see Figure S5 in the Supporting Information and Figure 4). The introduction of electron-rich substituents on the π system induces a reduction of the HOMO–LUMO gap by a pronounced increase of the HOMO energy level of **3b**, whereas the introduction of electron-withdrawing groups (**3c**) stabilizes in a similar manner the HOMO and LUMO levels inducing no reduction of the HOMO–LUMO gap (see Figure S5 in the Supporting Information). All these assumptions are nicely supported by the optical and electrochemical data.

Cyclic voltammetry, recorded in CH_2Cl_2 using Bu_4NPF_6 as electrolyte, was used to investigate the redox properties of **3a**–**f**, **4a**, and **5a** (Table 2). Compounds **3**–**5a** display different electrochemical behaviors depending on the P substitution. Compound **3a** presents only an irreversible electronic reduction wave ($E^o_{red\,1}=-2.19$ V vs. Fc^+/Fc) in the electrochemical window. On replacing O by S in **4a**, an irreversible electronic oxidation wave is observed ($E^o_{ox\,1}=+1.03$ V vs. Fc^+/Fc) and the reduction becomes reversible ($E^o_{red\,1}=-2.13$ V vs. Fc^+/Fc). Coordination to Au^I slightly modifies the potentials (see Table 2) while keeping the electrochemical gap constant (around 3.0 eV). All these observations demonstrate that chemical modifications performed at the P atom impact weakly the HOMO and LUMO energy of the phosphete compounds. As anticipated, introduction of electron-donating groups cathodically shifts the oxidation wave ($E^o_{ox\,1}=+0.76$ V vs. Fc^+/Fc for **3b**) whereas the introduction of electron-withdrawing groups anodically shifts the reduction wave ($E^o_{red\,1}=-1.87$ V vs. Fc^+/Fc for **3c**). Furthermore, the introduction of emissive subunits, such as fluorene (**3d**), naphthalene (**3e**), or carbazole (**3f**), also affects the redox potential. For example, compound **3d** displays amphoteric redox character with quasi-reversible electrochemical waves (see Table 2), which makes it appealing for application in optoelectronic devices. This study clearly shows that modifications of both the π-conjugated system and P environment impact the electrochemical properties of the compounds and allow fine-tuning of the band gap.

Interestingly, dihydrophosphete derivatives **3a**–**f** and **4a** display excellent thermal stability (Table 2). Thermogravimetric

Table 3. EL performance of devices as a function of the device structure and the doping rate.

Device[a]	EML[b] Doping rate [wt.%]	λ_{max}^{EL} [nm]	External quantum efficiency [%]	Current efficiency[c] [cd A^{-1}]	Power efficiency[c] [lm W^{-1}]	CIE coordinates *x*, *y*
A	**3d**	468/505	0.9	2.2	0.6	0.27, 0.46
B	CBP:**3d** (2.5%)	492	0.7	1.3	0.4	0.17, 0.32
C	DPVBi:**3d** (2.5%)	492	2.5	5.1	1.4	0.18, 0.34
D	CBP:**3e** (2.7%)	476	0.4	0.6	0.2	0.16, 0.24
E	DPVBi:**3e** (1.3%)	474	1.6	2.8	0.8	0.17, 0.27
F	DPVBi:**3e** (2.3%)	480	1.4	2.6	0.7	0.18, 0.29
G	DPVBi:**3e** (7.2%)	484	1.1	2.3	0.7	0.20, 0.32
H	DPVBi:**3f** (1.6%)	488	1.2	2.3	0.6	0.18, 0.31
I	DPVBi:**3f** (4.0%)	500	1.1	2.4	0.7	0.20, 0.39
ref.	DPVBi	468	2.1	3.2	0.9	0.16, 0.22

[a] Device configuration (thickness): ITO/CuPc (10 nm)/α-NPB (50 nm)/EML (15 nm)/DPVBi (35 nm)/BCP (10 nm)/Alq_3 (50 nm)/LiF (1.2 nm)/Al (100 nm). [b] Emitting layer (EML) = P emitter, DPVBi or CBP as host. [c] Measured at 20 mA cm^{-2}.

analysis (TGA) measurements performed under nitrogen atmosphere show that the whole family of compounds display decomposition temperatures above 300 °C, which allows them to be used in "small-molecule" OLED technology. Particularly, fluorene-substituted compound **3d** shows a decomposition temperature at 10% weight loss (T_{d10}) of 375 °C. Differential scanning calorimetry (DSC) measurements show that their melting points (T_m) were in the range of 75–230 °C (Table 2). The formation of a glassy state of these derivatives after melting and cooling was evidenced (for example, T_g (**3d**): 127 °C). Further heating above the glass transition temperature T_g and cooling to 45 °C resulted in no further crystallization or melting behavior. The results indicate that these compounds present good morphological and thermal stabilities, two critical issues for operating stability and lifetime of the devices.

The derivatives **3d–f** (Scheme 1) are thermally stable and emissive (Table 2), so they can be used as emitters in multilayer OLEDs. First, compound **3d** was used as a pure emitting layer (EML) in multilayer OLED **A** (Table 3), which has an indium tin oxide (ITO)/copper phthalocyanine (CuPc; 10 nm)/*N*,*N*′-diphenyl-*N*,*N*′-bis(1-naphthylphenyl)-1,1′-biphenyl-4,4′-diamine (α-NPB; 50 nm)/EML (15 nm)/4,4′-bis(2,2′-diphenylvinyl)biphenyl (DPVBi; 35 nm)/bathocuproine (BCP; 10 nm)/tris(8-hydroxyquinolinato)aluminum (Alq_3; 50 nm)/LiF (1.2 nm)/Al (100 nm) configuration (see Figure S6 in the Supporting Information). The electroluminescence (EL) spectrum of device **A** (λ_{maxEL} = 500 nm) resembles the thin-film PL spectrum of derivative **3d** (λ_{em} = 502 nm), thus showing that the EL emission bands are from this P luminophore. Furthermore, the increase of the current density does not impact the emission wavelength of device **A** (Figure 5), which proves that this emission is not due to degradation of the material. The luminance of this device reaches 1000 cd m^{-2} at 20 mA cm^{-2} with current and power efficiencies of 2.2 cd A^{-1} and 0.6 lm W^{-1}, respectively (Table 3). These moderate performances have been assigned to the moderate charge-carrier conduction properties of the EML. To improve the device performance, we incorporated the P fluorophore **3d** in two matrices having similar HOMO and LUMO energy levels but different charge-transport properties: 4,4′-bis(2,2′-diphenylvinyl)biphenyl (DPVBi) and 4,4′-*N*,*N*′-dicarbazole-biphenyl (CBP). CBP possesses a hole mobility at least one order of magnitude higher than its electron mobility[8] and DPVBi is usually used as blue emitter matrix and electron-transporting layer in OLEDs.[9] For a doping rate of 2.5%, the EL spectra of the devices **B** (CBP matrix) and **C** (DPVBi matrix) exhibit only the characteristic emission of the P derivative **3d**; no emission of the matrix is observed but the performance of these diodes is affected by the nature of the host material (Table 3). The device **C** using DPVBi as host exhibits much higher efficiencies than device **B** using the CBP matrix. Effectively, the external quantum efficiency, current and power efficiencies have been multiplied by about 4. This effect can be explained by a better charge transport as shown in Figure 6, in which the *J*–*V* curve for the device **C** comprising DPVBi as host is shifted to lower voltages comparatively to device **B** (CBP matrix). Furthermore, the performance of device **C** is very satisfying with a brightness of 3000 cd m^{-2} at 20 mA cm^{-2} (Figure S9 in the Supporting Information). Moreover, the brightness regularly increases with the current density (see the Supporting Information) showing the good stability of this OLED. A similar observation has been made with P fluorophore **3e** (Table 3, Figures S10 and S11 in the Supporting Information),

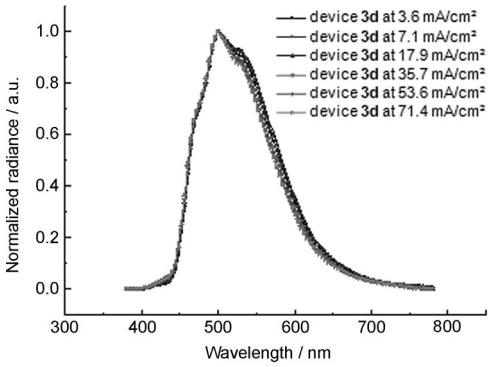

Figure 5. EL emission spectra of the diode **A** at different current densities.

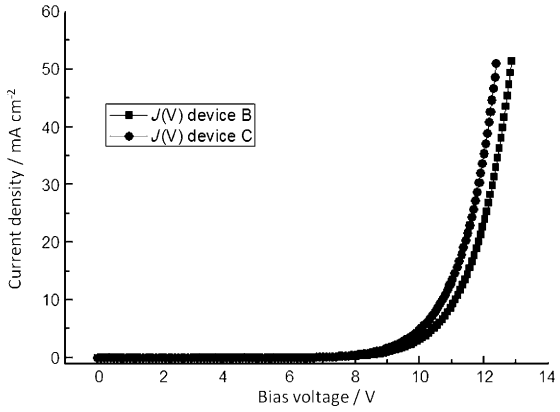

Figure 6. *J–V* characteristics of devices **B** and **C**.

only the EL emission maximum has been blueshifted (λ_{em} = 474 nm, Table 3) relative to device **C** due to the presence of the naphthalene substituents. As the device with DPVBi host had the best performance, we decided to keep the DPVBi matrix for studying the effect of the doping ratio on the EL performance when compounds **3e** and **3f** were used as emitters. As can be seen in Table 3 (devices **E**–**I**), the performance of the devices is not changed by an increase of the doping ratio. Even for a high doping ratio (device **G**) the quenching effect is limited due to the particular property of the P molecules avoiding the formation of strong aggregates.[3b] The increase of the doping rate induces only a small variation of the EL emission wavelength and on the International Commission on Illumination (CIE) coordinates.

In summary, all the P fluorophores present a greenish-blue emission. The best performance has been obtained for **3d** used as dopant in a DPVBi host (device **C**) with a current efficiency up to 5.1 cd A^{-1}, which is fairly good for a fluorescent blue emitter. Note that this value is higher than for the reference blue device with DPVBi as emitter (device **ref.**, Table 3).

Conclusion

The 1,2-dihydrophosphete skeleton is an interesting building block for the development of new π-conjugated oligomers. Variation of the substitution pattern of 1,2-dihydrophosphete derivatives and chemical modification of their P atoms afford thermally stable derivatives that are suitable emitters to construct efficient OLEDs. For example, OLEDs containing the phosphete-based compound **3d** as emitter exhibit blue electroluminescence, good performances, and current-independent CIE coordinates.

Experimental Section

General procedures

All experiments were performed under an atmosphere of dry nitrogen with standard Schlenk techniques. Column chromatography was performed in air, unless stated otherwise. Solvents were freshly distilled under nitrogen from sodium/benzophenone (tetrahydrofuran, diethyl ether) or from phosphorus pentoxide (dichloromethane, toluene). All reagents were used directly as received without further purification. Silica gel (200–300 mesh) for purification and silica gel TLC (F254) plates were purchased from Qing Dao Hai Yang Chemical Industry Co., China. ^{1}H, ^{13}C, and ^{31}P NMR spectra were recorded on a Bruker DPX-300 or Avance III-400 spectrometer. ^{1}H and ^{13}C NMR chemical shifts are reported in parts per million (ppm) relative to $Si(CH_3)_4$ as external standard. ^{31}P NMR downfield chemical shifts are expressed with a positive sign, in ppm, relative to external 85% H_3PO_4. High-resolution mass spectra were obtained on a Varian MAT 311, Waters Q-TOF 2, or ZabSpec TOF Micromass instrument at CRMPO, University of Rennes 1. Mass spectra of **1b**–**1f** were recorded on an LC-MSD-TRAP-XCT instrument by electrospray ionization (ESI). Elemental analyses were performed by the CRMPO, University of Rennes 1.

Determination of optical data

UV/Vis spectra were recorded at room temperature on a Varian Cary 5000 UV/Vis–near-IR spectrophotometer. Luminescence spectra were recorded at room temperature with an FS920 steady-state fluorimeter (M300, UC920, CD920/CD930, S900) using a xenon lamp (Xe900). All spectra were recorded in CH_2Cl_2 (SDS, HPLC grade) stabilized with ethanol, with concentrations of 5×10^{-6}, 1×10^{-5}, 5×10^{-5}, and 1×10^{-4} M. Quantum yields were calculated relative to quinine sulfate ($\Phi = 0.546$ in H_2SO_4 0.1 N)[10] by using the following equation: $Q_x/Q_r = [A_r(\lambda)/A_x(\lambda')][n_x^2/n_r^2][D_x/D_r]$ in which A is the absorbance at the excitation wavelength (λ), n the refractive index, and D the integrated luminescence intensity; "r" and "x" stand for reference and sample. Excitations of reference and sample compounds were performed at the maximum wavelength of the molecules.

Cyclic voltammetry measurements

The electrochemical studies were carried out under argon using an Eco Chemie Autolab PGSTAT 30 potentiostat for cyclic voltammetry with the three-electrode configuration: the working electrode was a platinum disk, the reference electrode a saturated calomel electrode, and the counter electrode a platinum wire. All potentials were internally referenced to the ferrocene/ferrocenium (Fc/Fc^+) couple. For the measurements, concentrations of 10^{-3} M of the electroactive species were used in freshly distilled and degassed dichloromethane (Lichrosolv, Merck) and 0.2 M tetrabutylammonium hexafluorophosphate (Fluka), which was twice recrystallized from ethanol and dried under vacuum prior to use.

Thermal analyses

Melting point and decomposition point determination were performed by using a differential scanning calorimeter (TA Instruments DSC Q20) and a thermogravimetric analyzer (TA Instruments TGA 2050) under dry nitrogen flow at a heating rate of 10 °C min^{-1}, respectively.

Device fabrication and characterization

Electroluminescent devices based on a multilayer structure were fabricated onto patterned ITO-coated glass substrates from XinYan Technology (thickness: 100 nm and sheet resistance: less than 20 Ω m^{-1}). The organic materials (from Aldrich and Lumtec) were deposited onto the ITO anode by sublimation under high vacuum ($< 10^{-6}$ Torr) at a rate of 0.2–0.3 nm s^{-1}. The common structure of all the devices was the following: a thin layer (10 nm thick) of

copper phthalocyanine (CuPc) was used as hole injection layer and *N*,*N*′-diphenyl-*N*,*N*′-bis(1-naphthylphenyl)-1,1′-biphenyl-4,4′-diamine (α-NPB, 50 nm) as hole transporting layer. The emitting layer consisted of a 15 nm thick film of pure phosphole derivatives or DPVBi (or CBP)-doped phosphole derivatives. The doped layer was obtained by co-evaporation of the two compounds and the doping rate was controlled by tuning the evaporation rate of each material. A thin layer of bathocuproine (BCP, 10 nm) was used as hole blocking layer, and tris(8-hydroxyquinolinato)aluminum (Alq_3, 10 nm) was used as electron-transporting layer. Finally, a cathode consisting of LiF (1.2 nm) capped with Al (100 nm) was deposited onto the organic stack. The entire device was fabricated in the same run without breaking the vacuum. In this study, the thicknesses of the different organic layers were kept constant for all the devices. The active area of the devices defined by the overlap of the ITO anode and the metallic cathode was 0.28 cm^2.

The current–voltage–luminance characteristics of the devices were measured with a regulated power supply (Laboratory Power Supply EA-PS 3032-10B) combined with a multimeter and a 1 cm^2 area silicon calibrated photodiode (Hamamatsu). The spectral emission was recorded with a SpectraScan PR655 spectrophotometer. All the measurements were performed at room temperature and under ambient atmosphere with no further encapsulation of devices immediately after the device realization.

Details of the X-ray crystallography study

Single-crystal data collection was performed at 100 K with an APEX II Bruker-AXS instrument (Centre de Diffractométrie, Université de Rennes 1, France) with $Mo_{K\alpha}$ radiation ($\lambda = 0.71073$ Å). Reflections were indexed, Lorentz-polarization corrected, and integrated by the DENZO program of the KappaCCD software package. The data merging process was performed using the SCALEPACK program.[11] Structure determinations were performed by direct methods with the solving program SIR97[12] that revealed all the non-hydrogen atoms. The SHELXL program (G. M. Sheldrick, SHELX97, Program for the Refinement of Crystal Structures, University of Göttingen, Germany, 1997) was used to refine the structures by full-matrix least-squares based on F^2. All non-hydrogen atoms were refined with anisotropic displacement parameters. Hydrogen atoms were included in idealized positions and refined with isotropic displacement parameters. Atomic scattering factors for all atoms were taken from International Tables for X-ray Crystallography.[13] Details of the crystal data and structural refinements are given in Table S2 in the Supporting Information.

CCDC 948792 contains the supplementary crystallographic data for this paper. These data can be obtained free of charge from The Cambridge Crystallographic Data Centre via www.ccdc.cam.ac.uk/data_request/cif.

Calculations on the phosphete derivatives

All the density functional calculations were carried out using the Gaussian 03 code. This level of the theory has provided satisfactory results for the phosphete oligomers.[14] The geometries were fully optimized, and vibrational analysis was performed on the optimized structures to check whether the stationary point located was a minimum of the potential energy hypersurface. The density functional theory (DFT) calculation and structure optimization of **2a** and **3a**–**c** were conducted at the B3LYP/6-31+G(d,p) level.

Experimental methods

Synthesis of 1a–f: Phenylbis(2-phenylethynyl)phosphine (**1a**) was prepared according to the previously reported procedure.[6] A similar procedure was used to prepare **1b**–**f**. The typical procedure is as follows: a mixture of terminal alkyne (12.8 mmol), $PhPCl_2$ (0.7 mL, 5.2 mmol), CuI (0.1 g, 0.52 mmol), NEt_3 (4.35 mL), and toluene (35 mL) was stirred at room temperature for 12 h. After filtration and removal of the solvent, the residue was chromatographed over silica gel (hexane) to give **1**.

Synthesis of 1b: Compound **1b** was obtained as a yellow solid (1.60 g, 4.3 mmol; yield: 83%). ^{31}P NMR ($CDCl_3$, 121 MHz): $\delta = -60.7$ ppm (s); ^1H NMR ($CDCl_3$, 300 MHz): $\delta = 3.82$ (s, 6H; OCH_3), 7.18 (AB system, $J_{AB} = 8.9$ Hz, $\Delta\nu_{AB} = 188.3$ Hz, 8H; $CH_{phenyl\text{-}OCH3}$), 7.44–7.51 (m, 3H; *CH*phenyl), 7.87–7.93 ppm (m, 2H; *CH*phenyl); ^{13}C NMR ($CDCl_3$, 75 MHz): $\delta = 55.3$ (s, OCH_3), 81.4 (s, *C*≡C), 106.5 (d, *J*(C,P) = 7.4 Hz, *C*≡C), 113.9 (s, *C*Hphenyl), 114.6 (s, *C*phenyl), 128.8 (d, *J*(C,P) = 7.6 Hz, *C*Hphenyl), 129.3 (s, *C*Hphenyl), 132.0 (d, *J*(C,P) = 21.8 Hz, *C*Hphenyl), 133.7 (d, *J*(C,P) = 1.5 Hz, *C*Hphenyl), 133.8 (s, *C*phenyl), 160.3 ppm (s, *C*phenyl); HRMS (ESI, MeOH): *m/z*: calcd for $C_{24}H_{19}O_2KP$: 409.07 $[M+K]^+$; found: 409.1.

Synthesis of 1c: Compound **1c** was obtained as a brown solid (1.09 g, 2.4 mmol; yield: 47%). ^{31}P NMR ($CDCl_3$, 121 MHz): $\delta = -61.6$ ppm (s); ^1H NMR ($CDCl_3$, 300 MHz): $\delta = 7.47$–7.50 (m, 3H; *CH*phenyl), 7.59–7.65 (m, 8H; *CH*phenyl), 7.86–7.92 ppm (m, 2H; *CH*phenyl); ^{13}C NMR ($CDCl_3$, 75 MHz): $\delta = 85.5$ (d, *J*(C,P) = 6.3 Hz, *C*≡C), 104.8 (d, *J*(C,P) = 6.4 Hz, *C*≡C), 123.8 (q, *J*(C,F) = 270.6 Hz, CF_3), 125.3 (q, *J*(C,F) = 3.7 Hz, *C*Hphenyl), 126.0 (s, *C*phenyl), 129.1 (d, *J*(C,P) = 8.2 Hz, *C*Hphenyl), 130.1 (s, *C*Hphenyl), 130.8 (q, *J*(C,F) = 32.6 Hz, *C*phenyl), 132.0 (s, *C*phenyl), 132.17 (d, *J*(C,P) = 1.6 Hz, *C*Hphenyl), 132.5 ppm (d, *J*(C,P) = 22.4 Hz, *C*Hphenyl); MS (ESI, MeOH): *m/z*: calcd for $C_{24}H_{13}F_6KP$: 485.03 $[M+K]^+$; found: 485.0.

Synthesis of 1d: Compound **1d** was obtained as a white solid (1.38 g, 2.5 mmol; yield: 49%). ^{31}P NMR ($CDCl_3$, 121 MHz): $\delta = -60.7$ ppm (s); ^1H NMR ($CDCl_3$, 300 MHz): $\delta = 1.65$ (s, 12H; CH_3), 7.50–7.90 (m, 17H; *CH*phenyl), 8.32 ppm (t, *J*(H,H) = 8.4 Hz, *J*(H,P) = 8.4 Hz, 2H; *CH*phenyl); ^{13}C NMR ($CDCl_3$, 75 MHz): $\delta = 27.2$ (s, CH_3), 47.1 (s, $C(CH_3)_2$), 83.3 (s, *C*≡C), 107.8 (d, *J*(C,P) = 7.4 Hz, *C*≡C), 120.3 (s, *C*Hphenyl), 120.8 (s, *C*Hphenyl), 121.1 (s, *C*phenyl), 123.0 (s, *C*Hphenyl), 126.7 (s, *C*Hphenyl), 127.5 (s, *C*Hphenyl), 128.3 (s, *C*Hphenyl), 129.3 (d, *J*(C,P) = 7.8 Hz, *C*Hphenyl), 129.9 (s, *C*Hphenyl), 131.7 (s, *C*Hphenyl), 132.6 (d, *J*(C,P) = 21.8 Hz, *C*Hphenyl), 133.8 (s, *C*phenyl), 138.5 (s, *C*phenyl), 140.6 (s, *C*phenyl), 153.8 (s, *C*phenyl), 154.2 ppm (s, *C*phenyl); MS (ESI, MeOH): *m/z*: calcd for $C_{40}H_{32}P$: 543.2 $[M+H]^+$; found: 543.2.

Synthesis of 1e: Compound **1e** was obtained as a white solid (1.77 g, 4.3 mmol; yield: 83%). ^{31}P NMR ($CDCl_3$, 121 MHz): $\delta = -60.8$ ppm (s); ^1H NMR ($CDCl_3$, 300 MHz): $\delta = 7.49$–7.68 (m, 9H; C*H*aromatic), 7.89–7.94 (m, 6H; C*H*aromatic), 8.22 (t, *J*(H,H) = 8.4 Hz, *J*(H,P) = 9.0 Hz, 2H; C*H*aromatic), 8.56 ppm (d, *J*(H,H) = 8.1 Hz, 2H; C*H*aromatic); ^{13}C NMR ($CDCl_3$, 75 MHz): $\delta = 88.3$ (d, *J*(C,P) = 4.5 Hz, *C*≡C), 104.8 (d, *J*(C,P) = 6.8 Hz, *C*≡C), 120.2 (s, *C*aromatic), 125.3 (s, *C*Haromatic), 126.2 (s, *C*Haromatic), 126.7 (s, *C*Haromatic), 127.3 (s, *C*Haromatic), 128.5 (s, *C*Haromatic), 129.2 (d, *J*(C,P) = 8.0 Hz, *C*Haromatic), 129.9 (s, *C*Haromatic), 131.3 (d, *J*(C,P) = 1.7 Hz, *C*Haromatic), 132.4 (s, *C*Haromatic), 132.7 (s, *C*Haromatic), 133.2 (s, *C*aromatic), 133.5 (s, *C*aromatic), 133.6 ppm (s, *C*aromatic); MS (ESI, MeOH): *m/z*: calcd for $C_{30}H_{20}P$: 411.5 $[M+H]^+$; found: 411.3.

Synthesis of 1 f: Compound **1 f** was obtained as a white solid (2.02 g, 3.2 mmol; yield: 62%). ^{31}P NMR ($CDCl_3$, 121 MHz): $\delta = -61.4$ ppm (s); ^{1}H NMR ($CDCl_3$, 300 MHz): $\delta = 0.90$ (t, J(H,H) = 6.9 Hz, 6H; CH_3), 1.35–1.38 (m, 8H; CH_2), 1.85–1.89 (m, 4H; CH_2), 4.28 (t, J(H,H) = 7.2 Hz, 4H; N-CH_2), 7.26–7.55 (m, 11H; C*H*phenyl), 7.67 (dd, J(H,H) = 1.2, 8.4 Hz, 2H; C*H*phenyl), 8.03–8.05 (m, 2H; C*H*phenyl), 8.09 (d, J(H,H) = 7.8 Hz, 2H; C*H*phenyl), 8.34 ppm (s, 2H; C*H*phenyl); ^{13}C NMR ($CDCl_3$, 75 MHz): $\delta = 14.1$ (s, CH_3), 22.6 (s, CH_2), 28.8 (s, CH_2), 29.4 (s, CH_2), 43.2 (s, CH_2), 80.9 (s, C≡C), 108.3 (d, J(C,P) = 7.7 Hz, C≡C), 108.8 (s, *C*Hphenyl), 109.1 (s, *C*Hphenyl), 112.5 (s, *C*phenyl), 119.6 (s, *C*Hphenyl), 120.6 (s, *C*Hphenyl), 122.5 (s, *C*phenyl), 122.8 (s, *C*phenyl), 124.9 (s, *C*Hphenyl), 126.3 (s, *C*Hphenyl), 128.9 (d, J(C,P) = 7.5 Hz, *C*Hphenyl), 129.3 (s, *C*Hphenyl), 129.8 (s, *C*Hphenyl), 132.2 (d, J(C,P) = 21.2 Hz, *C*Hphenyl), 134.6 (s, *C*phenyl), 140.6 (s, *C*phenyl), 140.8 ppm (s, *C*phenyl); MS (ESI, MeOH): *m/z*: calcd for $C_{44}H_{42}N_2P$: 629.8 $[M+H]^+$; found: 629.6.

Synthesis of 3 a: Bromobenzene (312 μL, 3.0 mmol) was added to a distilled ether solution (20 mL) containing an excess of Mg (86 mg, 3.6 mmol) at room temperature. After 1 h of stirring at 40 °C, Cp_2ZrCl_2 (292 mg, 1.0 mmol) was introduced into the solution. The solution was stirred until complete dissolution of the solid, then dioxane (258 μL, 3.0 mmol) was added generating a white precipitate. The mixture was stirred for 1 h at room temperature and the solvent was evaporated under vacuum. The white solid was dissolved in degassed toluene (20 mL) and phenylbis(2-phenylethynyl)phosphine **1 a** (293 mg, 0.95 mmol) was added. After 20 h of stirring at 80 °C, a solution of toluene (20 mL) charged with HCl gas (from $NH_4Cl + H_2SO_4$) was added to the mixture at 0 °C. After 1 h of stirring at room temperature, the solution was filtered and the solvent was removed under vacuum. The crude residue was dissolved in CH_2Cl_2 (10 mL) and an excess of H_2O_2 (5 mL) was added. After 1 h of stirring at room temperature, water (10 mL) was added to the reaction mixture and the aqueous layer was extracted with CH_2Cl_2 (3×5 mL). The organic layer was dried over anhydrous $MgSO_4$ and the solvent was evaporated under vacuum. The crude product was purified by chromatography on silica (petroleum ether/AcOEt, 2:1, *v/v*). The recovered fraction was crystallized in Et_2O to give a pure white solid in 56% yield (215 mg, 0.53 mmol). ^{31}P NMR ($CDCl_3$, 121 MHz): $\delta = +35.6$ ppm (s); ^{1}H NMR ($CDCl_3$, 300 MHz): $\delta = 7.23$–7.63 (m, 18H; C*H*phenyl), 7.89 (d, J(H,P) = 70.5 Hz, 1H; =C*H*), 7.87 ppm (dd, J(H,P) = 12.0 Hz, J(H,H) = 7.5 Hz, 2H; C*H*phenyl); ^{13}C NMR ($CDCl_3$, 75 MHz): $\delta = 127.2$ (d, J(C,P) = 8.9 Hz, *C*Hphenyl), 128.3 (s, *C*Hphenyl), 128.4 (s, *C*Hphenyl), 128.5 (s, *C*Hphenyl), 128.6 (s, *C*Hphenyl), 128.9 (s, *C*Hphenyl), 129.0 (d, J(C,P) = 11.9 Hz, *C*Hphenyl), 129.1 (s, *C*Hphenyl), 129.8 (s, *C*Hphenyl), 129.9 (s, *C*Hphenyl), 130.7 (d, J(C,P) = 85.1 Hz, *C*ipso), 131.0 (d, J(C,P) = 5.8 Hz, *C*phenyl), 131.2 (d, J(C,P) = 11.3 Hz, *C*Hphenyl), 132.5 (d, J(C,P) = 2.7 Hz, *C*Hphenyl), 139.3 (d, J(C,P) = 8.8 Hz, *C*phenyl), 139.4 (d J(C,P) = 16.9 Hz, *C*sp^2), 140.0 (s, *C*phenyl), 142.1 (d, J(C,P) = 77.0 Hz, *C*sp^2), 144.7 (d, J(C,P) = 12.5 Hz, =*C*H), 155.7 ppm (d, J(C,P) = 78.4 Hz, *C*sp^2); HRMS (ESI, $CHCl_3$/MeOH, 50:50, *v/v*): *m/z*: calcd for $C_{28}H_{21}ONaP$: 427.12277 $[M+Na]^+$; found: 427.1228; elemental analysis calcd (%) for $C_{28}H_{21}OP$ (404.45): C 83.15, H 5.23; found: C 82.37, H 5.24.

Synthesis of 4 a: The procedure was similar to that for **3 a**. Instead of adding H_2O_2, S_8 (38 mg, 1.2 mmol) was added. The mixture was stirred for 12 h at 50 °C. The crude residue was purified by column chromatography on silica with petroleum ether/CH_2Cl_2 (1:1) as eluent. The product was obtained as a pale yellow solid in 54% yield (215 mg, 0.51 mmol). ^{31}P NMR ($CDCl_3$, 121 MHz): $\delta = +57.3$ ppm (s); ^{1}H NMR ($CDCl_3$, 300 MHz): $\delta = 7.03$–7.43 (m, 18H; C*H*phenyl), 7.69 (d, J(H,P) = 69.9 Hz, 1H; =C*H*), 7.94 ppm (ddd, J(H,P) = 14.1 Hz, J(H,H) = 7.8, 1.5 Hz, 2H; C*H*phenyl); ^{13}C NMR ($CDCl_3$, 75 MHz): $\delta = 126.8$ (d, J(C,P) = 9.2 Hz, *C*Hphenyl), 128.1 (s, *C*Hphenyl), 128.4 (s, *C*Hphenyl), 128.5 (s, *C*Hphenyl), 128.6 (s, *C*Hphenyl), 128.9 (s, *C*Hphenyl), 129.0 (s, *C*Hphenyl), 129.6 (s, *C*Hphenyl), 129.9 (s, *C*Hphenyl), 130.1 (s, *C*Hphenyl), 130.7 (d, J(C,P) = 6.2 Hz, *C*phenyl), 130.8 (d, J(C,P) = 64.8 Hz, *C*ipso), 131.4 (d, J(C,P) = 12.2 Hz, *C*Hphenyl), 132.4 (d, J(C,P) = 3.0 Hz, *C*Hphenyl), 138.6 (d, J(C,P) = 8.3 Hz, *C*phenyl), 139.2 (d, J(C,P) = 16.7 Hz, *C*sp^2), 139.3 (s, *C*phenyl), 140.2 (d, J(C,P) = 67.2 Hz, *C*sp^2), 143.6 (d, J(C,P) = 12.2 Hz, =*C*H), 153.1 ppm (d, J(C,P) = 68.6 Hz, *C*sp^2); HRMS (ESI, $CHCl_3$/MeOH, 50:50, *v/v*): *m/z*: calcd for $C_{28}H_{21}SNaP$: 443.09993 $[M+Na]^+$; found: 443.0999; elemental analysis calcd (%) for $C_{28}H_{21}PS$ (420.51): C 79.98, H 5.03, S 7.63; found: C 80.01, H 5.00, S 7.66.

Synthesis of 5 a: The procedure was similar to that for **3 a**. Instead of adding H_2O_2, (tht)AuCl (tht = tetrahydrothiophene; 256 mg, 0.8 mmol) was added and the mixture was stirred for 1 h. After solvent evaporation, the crude residue was purified by column chromatography on silica with petroleum ether/CH_2Cl_2 (2:1) as eluent. Further purification by crystallization in CH_2Cl_2/hexane was possible. The product was obtained as pale yellow crystals in 34% yield (203 mg, 0.32 mmol). ^{31}P NMR ($CDCl_3$, 121 MHz): $\delta = +49.6$ ppm (s); ^{1}H NMR ($CDCl_3$, 300 MHz): $\delta = 7.07$–7.42 (m, 18H; C*H*phenyl), 7.61 (ddd, J(H,P) = 14.1 Hz, J(H,H) = 8.7, 1.5 Hz, 2H; C*H*phenyl), 7.67 ppm (d, J(H,P) = 51.6 Hz, 1H; =C*H*); ^{13}C NMR ($CDCl_3$, 75 MHz): $\delta = 126.3$ (d, J(C,P) = 8.9 Hz, *C*Hphenyl), 127.7 (d, J(C,P) = 43.9 Hz, *C*ipso), 128.4 (s, *C*Hphenyl), 128.9 (s, *C*Hphenyl), 129.0 (d, J(C,P) = 12.8 Hz, *C*Hphenyl), 129.2 (s, *C*Hphenyl), 129.4 (d, J(C,P) = 11.9 Hz, *C*Hphenyl), 129.6 (s, *C*Hphenyl), 129.8 (s, *C*Hphenyl), 130.3 (s, *C*Hphenyl), 130.8 (d, J(C,P) = 7.3 Hz, *C*phenyl), 130.9 (d, J(C,P) = 57.4 Hz, *C*ipso), 133.3 (s, *C*Hphenyl), 133.4 (d, J(C,P) = 14.3 Hz, *C*Hphenyl), 138.3 (d, J(C,P) = 14.1 Hz, *C*sp^2), 138.4 (d, J(C,P) = 7.5 Hz, *C*phenyl), 141.4 (s, *C*phenyl), 143.0 (d, J(C,P) = 7.2 Hz, =*C*H), 147.5 ppm (d, J(C,P) = 52.1 Hz, *C*sp^2); HRMS (ESI, CH_3OCH_3): *m/z*: calcd for $C_{28}H_{21}ClAuNaP$: 643.06327 $[M+Na]^+$; found: 643.0632; elemental analysis calcd (%) for $C_{28}H_{21}AuClP$ (620.87): C 54.17, H 3.41; found: C 54.49, H 3.28.

Synthesis of 3 b: The procedure was similar to that for **3 a**. The crude residue was purified by column chromatography on silica (petroleum ether/AcOEt, 1:1) and recrystallization in absolute ethanol to afford the product in 45% yield (200 mg, 0.43 mmol). ^{31}P NMR ($CDCl_3$, 121 MHz): $\delta = 34.4$ ppm (s); ^{1}H NMR ($CDCl_3$, 300 MHz): $\delta = 3.69$ (s, 3H; OCH_3), 3.70 (s, 3H; OCH_3), 6.73 (d, J(H,H) = 8.7 Hz, 2H; C*H*phenyl), 6.79 (d, J(H,H) = 8.4 Hz, 2H; C*H*phenyl), 7.30–7.43 (m, 12H; C*H*phenyl), 7.70 (d, J(H,P) = 71.4 Hz, 1H; =C*H*), 7.88 ppm (dd, J(H,P) = 11.4 Hz, J(H,H) = 7.5 Hz, 2H; C*H*phenyl); ^{13}C NMR ($CDCl_3$, 75 MHz): $\delta = 55.2$ (s, O*C*H$_3$), 55.3 (s, O*C*H$_3$), 113.8 (s, *C*Hphenyl), 114.5 (s, *C*Hphenyl), 123.9 (d, J(C,P) = 6.0 Hz, *C*phenyl), 128.1 (s, *C*Hphenyl), 128.5 (s, *C*Hphenyl), 128.7 (d, J(C,P) = 9.0 Hz, *C*Hphenyl), 129.0 (d, J(C,P) = 12 Hz, *C*Hphenyl), 129.9 (s, *C*Hphenyl), 130.2 (s, *C*Hphenyl), 130.8 (d, J(C,P) = 86.3 Hz, *C*ipso), 131.2 (d, J(C,P) = 11.3 Hz, *C*Hphenyl), 132.0 (d, J(C,P) = 9.0 Hz, *C*phenyl), 132.4 (d, J(C,P) = 3.0 Hz, *C*Hphenyl), 138.4 (d, J(C,P) = 1.5 Hz, *C*phenyl), 139.7 (d, J(C,P) = 17.3 Hz, *C*sp^2), 140.2 (d, J(C,P) = 77.3 Hz, *C*sp^2), 142.3 (d, J(C,P) = 12.0 Hz, =*C*H), 154.1 (d, J(C,P) = 78.0 Hz, *C*sp^2), 159.7 (s, *C*phenyl), 160.8 ppm (s, *C*phenyl); HRMS (ESI, $CHCl_3$/MeOH, 50:50, *v/v*): *m/z*: calcd for $C_{30}H_{25}O_3NaP$: 487.1439 $[M+Na]^+$; found: 487.1440; elemental analysis calcd (%) for $C_{30}H_{25}O_3P$ (464.49): C 77.57, H 5.43; found: C 77.50, H 5.30.

Synthesis of 3c: The procedure was similar to that for **3a**. The crude residue was purified by column chromatography on silica with dichloromethane as eluent. The product was obtained as a yellow solid in 35% yield (180 mg, 0.33 mmol). ^{31}P NMR ($CDCl_3$, 121 MHz): $\delta = +35.4$ ppm (s); ^{1}H NMR ($CDCl_3$, 300 MHz): $\delta = 7.20$–7.23 (m, 2H; C*H*phenyl), 7.35–7.47 (m, 14H; C*H*phenyl), 7.75 (ddd, J(H,P) = 12.6 Hz, J(H,H) = 6.9, 1.8 Hz, 2H; C*H*phenyl), 7.90 ppm (d, J(H,P) = 69.0 Hz, 1H; =C*H*); ^{13}C NMR ($CDCl_3$, 75 MHz): $\delta = 123.7$ (q, J(C,F) = 270.5 Hz, *C*F3), 123.9 (q, J(C,F) = 270.5 Hz, *C*F3), 125.4 (q, J(C,F) = 3.5 Hz, *C*Hphenyl), 126.0 (q, J(C,F) = 3.8 Hz, *C*Hphenyl), 127.4 (d, J(C,P) = 8.6 Hz, *C*Hphenyl), 128.8 (s, *C*Hphenyl), 128.9 (s, *C*Hphenyl), 129.3 (d, J(C,P) = 12.2 Hz, *C*Hphenyl), 129.4 (s, *C*Hphenyl), 129.8 (s, *C*Hphenyl), 130.3 (q, J(C,F) = 32.2 Hz, *C*phenyl), 130.6 (d, J(C,P) = 86.1 Hz, *C*ipso), 131.2 (d, J(C,P) = 11.4 Hz, *C*Hphenyl), 131.4 (q, J(C,F) = 32.5 Hz, *C*phenyl), 133.0 (d, J(C,P) = 2.8 Hz, *C*Hphenyl), 134.0 (d, J(C,P) = 6.0 Hz, *C*phenyl), 138.4 (d, J(C,P) = 16.4 Hz, *C*sp^2), 140.2 (s, *C*phenyl), 142.6 (d, J(C,P) = 8.2 Hz, *C*phenyl), 143.5 (d, J(C,P) = 76.5 Hz, *C*sp^2), 146.7 (d, J(C,P) = 11.8 Hz, =*C*H), 155.3 ppm (d, J(C,P) = 78.5 Hz, *C*sp^2); HRMS (ESI, $CHCl_3$/MeOH, 50:50, *v/v*): *m/z*: calcd for $C_{30}H_{19}OF_6NaP$: 563.09754 $[M+Na]^+$; found: 563.0977; elemental analysis calcd (%) for $C_{30}H_{19}OF_6P$ (540.446): C 66.67, H 3.54; found: C 66.81, H 3.40.

Synthesis of 3d: The procedure was similar to that for **3a**. The crude residue was purified by column chromatography on silica with petroleum ether/AcOEt (3:1, *v/v*) as eluent. The product was obtained as a yellow solid (278 mg, 0.44 mmol, 46% yield). ^{31}P NMR ($CDCl_3$, 121 MHz): $\delta = +36.0$ ppm (s); ^{1}H NMR ($CDCl_3$, 300 MHz): $\delta = 1.46$ (s, 3H; CH_3), 1.49 (s, 3H; CH_3), 1.53 (s, 3H; CH_3), 1.56 (s, 3H; CH_3), 7.19 (d, J(H,H) = 8.1 Hz, 1H; C*H*aromatic), 7.27–7.73 (m, 20H; C*H*aromatic), 7.99 (d, J(H,P) = 70.8 Hz, 1H; =C*H*), 8.01–8.07 ppm (m, 3H; C*H*aromatic); ^{13}C NMR ($CDCl_3$, 75 MHz): $\delta =$ 26.9 (s, *C*H$_3$), 27.0 (s, *C*H$_3$), 27.1 (s, *C*H$_3$), 27.2 (s, *C*H$_3$), 46.9 (s, *C*fluorenyl), 47.0 (s, *C*fluorenyl), 119.7 (s, *C*Haromatic), 120.3 (s, *C*Haromatic), 120.5 (s, *C*Haromatic), 120.6 (s, *C*Haromatic), 120.9 (d, J(C,P) = 9.5 Hz, *C*Haromatic), 122.7 (s, *C*Haromatic), 123.2 (s, *C*Haromatic), 126.8 (d, J(C,P) = 8.6 Hz, *C*Haromatic), 127.1 (s, *C*Haromatic), 127.3 (s, *C*Haromatic), 127.6 (s, *C*Haromatic), 128.1 (s, *C*Haromatic), 128.3 (s, *C*Haromatic), 128.6 (s, *C*Haromatic), 128.7 (s, *C*Haromatic), 129.1 (d, J(C,P) = 12.0 Hz, *C*Haromatic), 130.2 (s, *C*Haromatic), 130.9 (d, J(C,P) = 83.4 Hz, *C*ipso), 131.4 (d, J(C,P) = 11.3 Hz, *C*Haromatic), 132.5 (s, *C*Haromatic^2), 138.3 (s, *C*aromatic), 138.5 (d, J(C,P) = 8.6 Hz, *C*aromatic), 138.7 (s, *C*aromatic), 139.6 (s, *C*aromatic), 139.8 (d, J(C,P) = 16.9 Hz, *C*aromatic), 140.1 (s, *C*aromatic), 141.2 (s, *C*aromatic), 141.7 (d, J(C,P) = 77.0 Hz, *C*sp^2), 144.0 (d, J(C,P) = 12.4 Hz, =*C*H), 154.1 (d, J(C,P) = 8.0 Hz, *C*aromatic), 154.4 (s, *C*aromatic), 155.6 ppm (d, J(C,P) = 78.5 Hz, *C*sp^2); one *C*Haromatic and three *C*aromatic are not observed, may overlap; HRMS (ESI, $CHCl_3$/MeOH, 50:50, *v/v*): *m/z*: calcd for $C_{46}H_{37}ONaP$: 659.24797 $[M+Na]^+$; found: 659.2476; elemental analysis calcd (%) for $C_{46}H_{37}OP$ (636.76): C 86.77, H 5.86; found: C 86.59, H 5.67.

Synthesis of 3e: The procedure was similar to that for **3a**. The crude product was purified by chromatography on silica (petroleum ether/AcOEt, 2:1). The recovered fraction was crystallized in Et_2O and hexane to give a yellow solid (277 mg, 0.55 mmol, 58% yield). ^{31}P NMR ($CDCl_3$, 121 MHz): $\delta = +36.4$ ppm (s); ^{1}H NMR ($CDCl_3$, 300 MHz): $\delta = 7.03$–7.71 (m, 23H; C*H*aromatic), 8.49 (d, J(H,P) = 72.0 Hz, 1H; =C*H*), 8.63 ppm (d, J(H,H) = 8.4 Hz, 1H; C*H*aromatic); ^{13}C NMR ($CDCl_3$, 100 MHz): $\delta = 125.4$ (s, *C*Haromatic), 125.6 (s, *C*Haromatic), 125.8 (s, *C*Haromatic), 126.1 (s, *C*Haromatic), 126.2 (s, *C*Haromatic), 126.6 (s, *C*Haromatic), 127.5 (d, J(C,P) = 9.4 Hz, *C*Haromatic), 127.7 (s, *C*Haromatic), 128.3 (s, *C*Haromatic), 128.5 (s, *C*Haromatic), 128.6 (s, *C*Haromatic), 128.7 (s, *C*Haromatic), 128.8 (s, *C*Haromatic), 128.9 (s, *C*Haromatic), 129.0 (s, *C*Haromatic), 129.1 (s, *C*Haromatic), 129.5 (d, J(C,P) = 3.6 Hz, *C*aromatic), 130.6 (d, J(C,P) = 79.8 Hz, *C*ipso), 130.7 (s, *C*Haromatic), 131.1 (d, J(C,P) = 11.6 Hz, *C*Haromatic), 131.7 (s, *C*aromatic), 132.3 (s, *C*Haromatic), 133.9 (s, *C*aromatic), 134.1 (s, *C*aromatic), 136.8 (d, J(C,P) = 10.7 Hz, *C*aromatic), 138.5 (s, *C*aromatic), 140.0 (d, J(C,P) = 17.5 Hz, *C*sp^2), 144.7 (d, J(C,P) = 82.1 Hz, *C*sp^2), 146.5 (d, J(C,P) = 12.5 Hz, =*C*H), 157.2 ppm (d, J(C,P) = 73.4 Hz, *C*sp^2); one *C*aromatic is not observed, may overlap; HRMS (ESI, MeOH): *m/z*: calcd for $C_{36}H_{25}OPNa$: 527.15407 $[M+Na]^+$; found: 527.1538; elemental analysis calcd (%) for $C_{36}H_{25}OP$ (504.16): C 85.70, H 4.99; found: C 85.95, H 5.24.

Synthesis of 3f: The procedure was similar to that for **3a**. The crude product was purified by chromatography on silica (petroleum ether/AcOEt, 4:1, *v/v*). The recovered fraction was crystallized in Et_2O and hexane to give a yellow solid (315 mg, 0.44 mmol, 46% yield). ^{31}P NMR ($CDCl_3$, 121 MHz): $\delta = +34.6$ ppm (s); ^{1}H NMR ($CDCl_3$, 300 MHz): $\delta = 0.85$ (t, J(H,H) = 6.6 Hz, 3H; CH_3), 0.87 (t, J(H,H) = 6.6 Hz, 3H; CH_3), 1.31–1.35 (m, 8H; CH_2), 1.81–1.83 (m, 4H; CH_2), 4.22 (t, J(H,H) = 7.2 Hz, 4H; N-CH_2), 7.13–7.59 (m, 18H; C*H*aromatic), 7.80 (s, 1H; C$H_{aromatic}$), 7.90 (d, J(H,P) = 71.7 Hz, 1H; =C*H*) 7.97–8.18 ppm (m, 5H; C*H*aromatic); ^{13}C NMR ($CDCl_3$, 75 MHz): $\delta =$ 13.9 (s, *C*H$_3$), 13.9 (s, *C*H$_3$), 22.4 (s, *C*H$_2$), 22.5 (s, *C*H$_2$), 28.6 (s, *C*H$_2$), 28.7 (s, *C*H$_2$), 29.3 (s, *C*H$_2$), 29.4 (s, *C*H$_2$), 43.2 (s, 2*C*H$_2$), 108.5 (s, *C*Haromatic), 108.7 (s, *C*Haromatic), 109.0 (s, *C*Haromatic), 109.2 (s, *C*Haromatic), 118.9 (s, *C*Haromatic), 119.5 (s, *C*Haromatic), 119.6 (s, *C*Haromatic), 120.7 (s, *C*Haromatic), 120.8 (s, *C*Haromatic), 121.3 (s, *C*Haromatic), 122.5 (d, J(C,P) = 6.0 Hz, *C*aromatic), 122.7 (s, *C*aromatic), 122.8 (s, *C*aromatic), 123.0 (s, *C*aromatic), 123.3 (s, *C*aromatic), 125.0 (d, J(C,P) = 9.2 Hz, *C*Haromatic), 125.7 (s, *C*Haromatic), 126.2 (s, *C*Haromatic), 127.2 (s, *C*Haromatic), 127.9 (s, *C*Haromatic), 128.5 (s, *C*Haromatic), 129.0 (d, J(C,P) = 11.9 Hz, *C*Haromatic), 130.3 (s, *C*Haromatic), 130.8 (d, J(C,P) = 8.8 Hz, *C*aromatic), 131.5 (d, J(C,P) = 11.2 Hz, *C*Haromatic), 131.7 (d, J(C,P) = 83.5 Hz, *C*ipso), 132.2 (s, *C*Haromatic), 138.9 (s, *C*aromatic), 140.4 (s, *C*aromatic), 140.5 (d, J(C,P) = 80.1 Hz, *C*sp^2), 140.6 (d, J(C,P) = 17.3 Hz, *C*sp^2), 140.8 (s, *C*aromatic), 141.0 (s, *C*aromatic), 141.9 (d, J(C,P) = 12.9 Hz, =*C*H), 155.2 ppm (d, J(C,P) = 78.1 Hz, *C*sp^2); one *C*aromatic not observed, may overlap; HRMS (ESI, CH_2Cl_2/MeOH, 10:90, *v/v*): *m/z*: calcd for $C_{50}H_{47}ON_2PNa$: 745.33182 $[M+Na]^+$; found: 745.3316; elemental analysis calcd (%) for $C_{50}H_{47}ON_2P$ (722.34): C 83.07, H 6.55; found: C 83.25, H 6.24.

Acknowledgements

This work was supported by the Ministère de la Recherche et de l'Enseignement Supérieur, the Institut Universitaire de France, the CNRS, the Région Bretagne, China-French associated international laboratory in "Functional Organophosphorus Materials" COST CM0802 (Phoscinet) and COST CM10302 (SIPS), the National Natural Science Foundation of China (21072179, 21272218), Henan Science and Technology Department (114300510007), and Zhengzhou Science and Technology Department (131PYSGZ204). The authors are grateful to C. Lescop for X-ray diffraction studies and to J. Troles for the DSC measurements.

Keywords: luminescence · molecular engineering · organic light-emitting diodes · phosphorus heterocycles · pi systems

[1] a) C. W. Tang, S. A. VanSlyke, *Appl. Phys. Lett.* **1987**, *51*, 913; b) C. Adachi, S. Tokito, T. Tsutsui, S. Saito, *Jpn J. Appl. Phys.* **1988**, *27*, L269; c) C. W. Tang, S. A. VanSlyke, C. H. Chen, *J. Appl. Phys.* **1989**, *65*, 3610; d) B. W. D'Andrade, S. R. Forrest, *Adv. Mater.* **2004**, *16*, 1585; e) K. T. Kamtekar, A. P. Monkman, M. R. Bryce, *Adv. Mater.* **2010**, *22*, 572; f) B. W. D'Andrade, *Nat. Photonics* **2007**, *1*, 33; g) M. C. Gather, A. Köhnen, K. Meerholz, *Adv. Mater.* **2011**, *23*, 233.

[2] a) P.-A. Bouit, A. Escande, R. Szűcs, D. Szieberth, C. Lescop, L. Nyulászi, M. Hissler, R. Réau, *J. Am. Chem. Soc.* **2012**, *134*, 6524; b) Y. Ren, W. H. Kan, M. A. Henderson, P. G. Bomben, C. P. Berlinguette, V. Thangadurai, T. Baumgartner, *J. Am. Chem. Soc.* **2011**, *133*, 17014; c) E. Deschamps, L. Ricard, F. Mathey, *Angew. Chem.* **1994**, *106*, 1214; *Angew. Chem. Int. Ed. Engl.* **1994**, *33*, 1158; d) Y. Matano, M. Nakashima, H. Imahori, *Angew. Chem.* **2009**, *121*, 4062; *Angew. Chem. Int. Ed.* **2009**, *48*, 4002; e) K. Yavari, S. Moussa, B. Ben Hassine, P. Retailleau, A. Voituriez, A. Marinetti, *Angew. Chem.* **2012**, *124*, 6852; *Angew. Chem. Int. Ed.* **2012**, *51*, 6748; f) W. Weymiens, M. Zaal, J. C. Slootweg, A. W. Ehlers, K. Lammertsma, *Inorg. Chem.* **2011**, *50*, 8516; g) Y. Dienes, M. Eggenstein, T. Kárpáti, T. C. Sutherland, L. Nyulászi, T. Baumgartner, *Chem. Eur. J.* **2008**, *14*, 9878; h) A. Fukazawa, M. Hara, T. Okamoto, E.-C. Son, C. Xu, K. Tamao, S. Yamaguchi, *Org. Lett.* **2008**, *10*, 913; i) A. Fukazawa, H. Yamada, S. Yamaguchi, *Angew. Chem.* **2008**, *120*, 5664; *Angew. Chem. Int. Ed.* **2008**, *47*, 5582.

[3] a) H. Chen, W. Delaunay, L. Yu, D. Joly, Z. Wang, J. Li, Z. Wang, C. Lescop, D. Tondelier, B. Geffroy, Z. Duan, M. Hissler, F. Mathey, R. Réau, *Angew. Chem.* **2012**, *124*, 218; *Angew. Chem. Int. Ed.* **2012**, *51*, 214; b) D. Joly, D. Tondelier, V. Deborde, W. Delaunay, A. Thomas, K. Bhanuprakash, B. Geffroy, M. Hissler, R. Réau, *Adv. Funct. Mater.* **2012**, *22*, 567; c) D. Joly, D. Tondelier, V. Deborde, B. Geffroy, M. Hissler, R. Réau, *New. J. Chem.* **2010**, *34*, 1603; d) O. Fadhel, M. Gras, N. Lemaitre, V. Deborde, M. Hissler, B. Geffroy, R. Réau, *Adv. Mater.* **2009**, *21*, 1261; e) H. Su, O. Fadhel, C.-J. Yang, T.-Y. Cho, C. Fave, M. Hissler, C.-C. Wu, R. Réau, *J. Am. Chem. Soc.* **2006**, *128*, 983.

[4] *Phosphorus-Carbon Heterocyclic Chemistry: The Rise of a New Domain*, (Ed.: F. Mathey), Pergamon, Oxford, 2001.

[5] a) A. Marinetti, J. Fischer, F. Mathey, *J. Am. Chem. Soc.* **1985**, *107*, 5001; b) N. H. Tran Huy, L. Richard, F. Mathey, *Organometallics* **1988**, *7*, 1791; c) H. Jun, R. J. Angelici, *Organometallics* **1993**, *12*, 4265; d) L. Weber, O. Kaminski, H.-G. Stammler, B. Neumann, *Organometallics* **1995**, *14*, 581; e) L. Dupuis, N. Pirio, P. Meunier, A. Igau, B. Donnadieu, J.-P. Majoral, *Angew. Chem.* **1997**, *109*, 1015; *Angew. Chem. Int. Ed. Engl.* **1997**, *36*, 987; f) N. Pirio, S. Bredeau, L. Dupuis, P. Schütz, B. Donnadieu, A. Igau, J.-P. Majoral, J.-C. Guillemin, P. Meunier, *Tetrahedron* **2004**, *60*, 1317; g) M. Zablocka, J. M. Majoral, *Current Org. Chem.* **2007**, *11*, 49.

[6] a) A. Hengefeld, R. Nast, *Chem. Ber.* **1983**, *116*, 2035; b) I. P. Beletskaya, V. V. Afanasiev, M. A. Kazankova, I. V. Efimova, *Org. Lett.* **2003**, *5*, 4309; c) V. V. Afanasiev, I. P. Beletskaya, M. A. Kazankova, I. V. Efimova, M.-U. Antipin, *Synthesis* **2003**, 2835.

[7] M. A. A. El-Bayoumi, F. M. A. Halim, *J. Chem. Phys.* **1968**, *48*, 2536.

[8] a) N. Matsusue, S. Ikame, Y. Suzuki, H. Naito, *Appl. Phys. Lett.* **2004**, *85*, 4046; b) H. I. Baek, C. Lee, *J. Appl. Phys.* **2008**, *103*, 054510.

[9] a) H. Choukri, A. Fischer, S. Forget, S. Chénais, M.-C. Castex, D. Adès, A. Siove, B. Geffroy, *Appl. Phys. Lett.* **2006**, *89*, 183513; b) E. I. Haskal, *Synth. Met.* **1997**, *91*, 187.

[10] J. N. Demas, G. A. Crosby, *J. Phys. Chem.* **1971**, *75*, 991.

[11] Z. Otwinowski, W. Minor in *Methods in Enzymology*, (Eds.: C. W. Carter, Jr., R. M. Sweet), Academic Press, New York, **1997**, 307.

[12] A. Altomare, M. C. Burla, M. Camalli, G. Cascarano, C. Giacovazzo, A. Guagliardi, A. G. G. Moliterni, G. Polidori, R. Spagna, *J. of Applied Cryst.* **1999**, *32*, 115.

[13] *International Tables for X-ray Crystallography, Vol. C* (Ed.: A. J. C. Wilson), Kluwer, Dordrecht, **1992**.

[14] Gaussian 03, Revision C.02, M. J. Frisch, G. W. Trucks, H. B. Schlegel, G. E. Scuseria, M. A. Robb, J. R. Cheeseman, J. A. Montgomery, Jr., T. Vreven, K. N. Kudin, J. C. Burant, J. M. Millam, S. S. Iyengar, J. Tomasi, V. Barone, B. Mennucci, M. Cossi, G. Scalmani, N. Rega, G. A. Petersson, H. Nakatsuji, M. Hada, M. Ehara, K. Toyota, R. Fukuda, J. Hasegawa, M. Ishida, T. Nakajima, Y. Honda, O. Kitao, H. Nakai, M. Klene, X. Li, J. E. Knox, H. P. Hratchian, J. B. Cross, C. Adamo, J. Jaramillo, R. Gomperts, R. E. Stratmann, O. Yazyev, A. J. Austin, R. Cammi, C. Pomelli, J. W. Ochterski, P. Y. Ayala, K. Morokuma, G. A. Voth, P. Salvador, J. J. Dannenberg, V. G. Zakrzewski, S. Dapprich, A. D. Daniels, M. C. Strain, O. Farkas, D. K. Malick, A. D. Rabuck, K. Raghavachari, J. B. Foresman, J. V. Ortiz, Q. Cui, A. G. Baboul, S. Clifford, J. Cioslowski, B. B. Stefanov, G. Liu, A. Liashenko, P. Piskorz, I. Komaromi, R. L. Martin, D. J. Fox, T. Keith, M. A. Al-Laham, C. Y. Peng, A. Nanayakkara, M. Challacombe, P. M. W. Gill, B. Johnson, W. Chen, M. W. Wong, C. Gonzalez, and J. A. Pople, Gaussian, Inc., Wallingford CT, 2004.

Received: January 6, 2014
Revised: February 21, 2014
Published online on July 2, 2014